2024 IEEE/ASME International Conference on Advanced Intelligent Mechatronics (AIM)
July 15-19, 2024. Boston, MA, USA

Dynamic Modeling and Design Optimization of an Artificial Muscle-Driven Limbless Robot for Agile Locomotion

Ayla Valles[1] and Mahdi Haghshenas-Jaryani[1]

***Abstract*— Future planetary explorations require versatile robots to adaptively traverse extreme access environments with optimal energy-consumption to address the current rovers' limitations. This paper discusses a study of the dynamics and velocity-based optimization for planar snake-robot muscle-driven locomotion. The system has two adjacent links connected by a pair of pneumatic artificial muscle (PAMs) series with extension springs. An alternate actuation of PAMs causes rotational motion about the connecting joint. The robot's kinematics in the joint and Cartesian space were derived with respect to the muscle motion. The robot's dynamic model were obtained for an N-Link system using Lagrangian mechanics. The performance of the dynamic model was then demonstrated through a MATLAB simulation for a two-link robot. Additionally, a velocity-based optimization was done to analyze the optimal linkage's geometric parameters and dynamical model properties that yields optimal forward velocity.**

I. INTRODUCTION

Animals have inspired roboticists to develop robotic systems with greater versatility and adaptability in their locomotion to address the challenges of conventional robots. Robots inspired by biological snakes have the potential to meet these growing needs. However, most snake-like robots developed over the last fifty years are made of rigid links actuated by either pneumatic actuators or electric motors. Having a short range of operation, low payload capacity, low agility, and high energy consumption. Unlike most conventional snake-like robots that used rotary shafts actuated by electric motors at the joint for forward propulsion, the MOIRA, developed by by Koichi Osuka and Hiroshi Kitajima [1], used two air cylinders acting as a joint driving actuator with a single fixed shaft producing little flexibility at each joint. The OmniTread design followed a similar concept using Pneumatic Bellows, one of the many pneumatic actuators that has been studied [2]. With emergence of soft robotics, it has become possible to create snake robots with more structurally deformable bodies that can perform complex motion with low cost, weight, and reduced complexity of the mechanical structures.

Pneumatic Artificial Muscles (PAMs) or "McKibben Muscle" have biomimetic behavior, self limiting factors, high power-to-weight ratio/force-to-volume ratio and energy efficiency highlight their advantageous in soft robotics [3]. However, disadvantages lie in their low bandwidth and non-optimal force models due to the hysteresis caused by Coulomb friction between the shape changing bladder and braids of the mesh cover. An inner tubing (bladder) with its elastic properties expands radially. The braided expandable sleeve serves to translate this radial expansion in to lateral contraction. On average PAMs contract 25% of their original length, although some have been shown to yield 40%. PAMs have also proven effective in energy consumption efficiency when compared to other soft actuators [3]–[5].

Recently PAMs have been used to replicate the musculoskeletal system of snakes considering the axial skeleton as a mechanical system comprised of a series of rigid rods hinged together and the axial musculature as a series of elastic elements (muscles) placed adjacent to the rod operating lateral to the hinges. The tension from the muscles acting antagonistically to each other generates potential energy to propel the snake forward. Gray's study of the biology and mechanics of a snake, mentions how a snake achieves serpentine movement or rather lateral undulation by sinusoidal propagation [6]–[10]. Whereas other snake-like robots with PAM actuators are fully soft with no rigid elements [11], [12], studies show the advantages a hybrid design has on improving the forward velocity.

In our previous work [13]–[15], PAM-driven snake robots were introduced. It was demonstrated through experimental and analytical studies that the kinematic and dynamic performances of the snake robot were promising, especially in low energy consumption, however, the forward velocity was only at 1.24 mm/s. With this new design, by adding extension springs we address the restricted movement and through dynamic optimization, we address improving the forward velocity of the previous design.

This work also presents the kinematics in the joint and Cartesian space derived with respect to the muscle motion. An extensive study on the dynamics for a planar muscle-driven spring series N-link snake robot was done using Lagrangian mechanics. A joint-torque controller was utilized to generate the relative muscle forces. Simulation studies were carried out using MATLAB on a model of a two-link system as the building block of the snake robot. Finally, a velocity-based design optimization was performed on the dynamic model for achieving optimal forward velocity.

II. KINEMATICS

The kinematics of robots is best described through the mapping between three configuration spaces, actuator, joint, and Cartesian/operational spaces. The interrelationship of the three spaces was studied for a muscle-driven snake robot

*This work is supported by a grant from NM NASA EPSCoR and New Mexico Space Grant Consortium (Grant Number: 80NSSC19M0181), and a grant from NASA (Grant Number: 80NSSC24K0839).

[1]Ayla Valles and Mahdi Haghshenas-Jaryani are with the Department of Mechanical and Aerospace Engineering, New Mexico State University, Las Cruces, NM 88003, USA aylav323@nmsu.edu and mahdihj@nmsu.edu

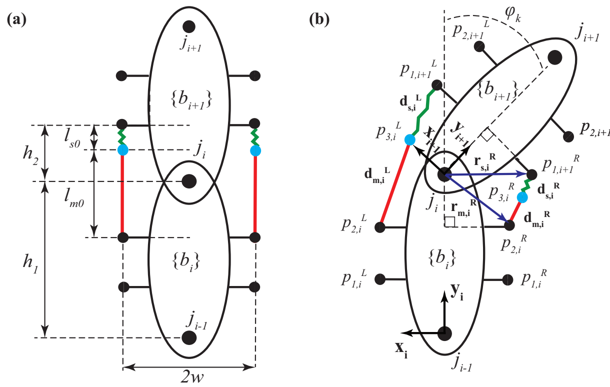

Fig. 1: Schematic of the artificial-muscle-driven snake robot kinematics, (a) geometry of the mechanism and (b) kinematics of the muscle length and the joint angle.

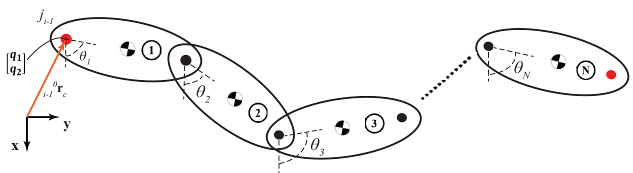

Fig. 2: Kinematics of a snake robot modeled as an articulated body with N moving links and N joints.

to develop kinematic models which were used in dynamic modeling and velocity-based design optimization.

A. Joint Position-Muscle Vector Relationship

The relationship between the joint position and the changing length of the muscle and spring was developed and studied. As illustrated in Fig. 1a, each muscle is coupled with a tension spring attached to two points on either side of a set of rigid links. To describe the motion of each muscle-spring coupling, vectors $\mathbf{d}_{m,i}$ and $\mathbf{d}_{s,i}$ on the right side are defined with respect to the body frame $\{b_i\}$ at the floating joint $\{j_{i-1}\}$ to form the *muscle-spring vector*, $\mathbf{d}_i$.

$$\mathbf{d}_i = \mathbf{d}_{m,i} + \mathbf{d}_{s,i} \tag{1}$$

This relation between the *muscle* and *spring vectors* considers the geometric parameters h_1, h_2, ω, ϕ_k, which are the length of each link, distance from the joint to the attachment point, half width of each link, and joint angle, as shown in Fig. 1a,b, respectively. Note that the joint angle is the orientation of the link $\{b_{i+1}\}$ with respect to the orientation of the previous link $\{b_i\}$.

B. Joint Space to Cartesian Space

The relationship between the joint space and the position and orientation of the moving links can be described by the forward kinematics of the planar snake robot as shown in Fig. 2. The Joint Space can be transformed to the Cartesian Space, where a link angle is introduced describing the robot's orientation with respect to a fixed reference frame $\{b_0\}$. The first joint is considered as a floating planar joint with two translational degrees-of-freedom (x, y) and one rotational DOF (link angle, θ_1), the remaining joints are one rotational DOF (joint angles). The link angle in relation to the joint angle where N is the number of links can be written as

$$\theta_i = \theta_1 + \sum_{k=1}^{i-1} \phi_k \qquad \{i = 2, \cdots, N\} \tag{2}$$

The connecting points $\mathbf{p}_{2,i}$ and $\mathbf{p}_{1,i+1}$ can then be rewritten with respect to the frame at joint j_{i-1}

$${}^{b_0}\mathbf{p}_{2,i} = \begin{bmatrix} x \\ y \end{bmatrix} + \sum_{k=1}^{i} ({}^{b_0}_{b_k}R \begin{bmatrix} w \\ h_1 - h_2 \end{bmatrix}) \tag{3}$$

$${}^{b_0}\mathbf{p}_{1,i+1} = \begin{bmatrix} x \\ y \end{bmatrix} + \sum_{k=1}^{i} ({}^{b_0}_{b_k}R \begin{bmatrix} w \\ h_2 \end{bmatrix}) \tag{4}$$

where ${}^{0}_{i}R$ is a rotation matrix of simple rotation about the Z axis of the joint. The *muscle-spring vector* is described by

$$\mathbf{d}_i = {}^{b_0}\mathbf{p}_{1,i+1} - {}^{b_0}\mathbf{p}_{2,i} \tag{5}$$

The relation between the lengths of the muscle, $l_{m,i}$ and spring, $l_{s,i}$ with the connecting points can be calculated as

$$l_{m,i} + l_{s,i} = \|{}^{b_0}\mathbf{p}_{2,i} - {}^{b_0}\mathbf{p}_{1,i+1}\| \tag{6}$$

The mass of the connecting point between the muscle and the spring is negligible therefore this point can be considered as massless, ${}^{b_0}\mathbf{p}_{3,i}$ with respect to the fixed reference frame. This point is not attached to a body like the previous points, and depending on the circumstance its position is calculated by three different methods. The first method states, when describing the motion of the snake robot with relation to its dynamics there are some instances when the length of the muscle which has become passive is said to be constant. If this is true the position of the point which joins the muscle to the spring, ${}^{b_0}\mathbf{p}_{3,i}$ can be calculated as

$${}^{b_0}\mathbf{p}_{3,i} = l_{m,0}\,\hat{\mathbf{e}}_i + {}^{b_0}\mathbf{p}_{2,i} \tag{7}$$

where $l_{m,0}$ and $\hat{\mathbf{e}}_i$ are the constant muscle length and unit vector of the *muscle-spring vector*, respectively.

The second method of ${}^{b_0}\mathbf{p}_{3,i}$ uses a similar equation as (7) where the length of the spring, $l_{s,i}$, is used instead. Notice how unlike in (7) where the initial muscle length is used, the changing length of the spring is now used.

$${}^{b_0}\mathbf{p}_{3,i} = -l_{s,i}\,\hat{\mathbf{e}}_i + {}^{b_0}\mathbf{p}_{1,i+1} \tag{8}$$

The last method, refers to the muscle becoming active on either side where there is both spring and opposing muscle forces which are of the same magnitude but opposite directions of each other acting on ${}^{b_0}\mathbf{p}_{3,i}$. In this analysis an assumption is made which states that the spring and muscle are always aligned with each other. Therefore, utilizing this balance of forces and the relation between the connecting points ${}^{b_0}\mathbf{p}_{2,i}$ and ${}^{b_0}\mathbf{p}_{3,i}$ for the length of the spring yields,

$$\|{}^{b_0}\mathbf{p}_{1,i+1} - {}^{b_0}\mathbf{p}_{3,i}\|^2 = (\frac{\|\mathbf{f}_{m,i}\|}{k} + l_{s,0})^2 \tag{9}$$

where $l_{s,i}, l_{s,0}, k, \mathbf{f}_{m,i}$ are the changing and initial spring lengths, spring constant, and muscle force respectively.

Solving (9) for the position vector ${}^{b_0}\mathbf{p}_{3,i}$ results in two unique solutions. The muscle lengths can be written as,

$$l_{m,i} = \|{}^{b_0}\mathbf{p}_{3,i} - {}^{b_0}\mathbf{p}_{2,i}\| \tag{10}$$

The previously mentioned rotation matrix in addition to translation vector, ${}^{b_i}\mathbf{r}_c$ is used to find the center of mass (CoM) of each rigid link described as

$${}^{b_0}\mathbf{p}_{C,i} = \begin{bmatrix} x \\ y \end{bmatrix} + \sum_{k=1}^{i-1}(2\,{}^{b_0}_{b_k}R\;{}^{b_k}\mathbf{r}_c) + {}^{b_0}_{b_i}R\;{}^{b_i}\mathbf{r}_c \tag{11}$$

where

$${}^{b_i}\mathbf{r}_c = \begin{bmatrix} 0 \\ \frac{h_1}{2} \end{bmatrix} \quad i = 1, 2, \cdots, N. \tag{12}$$

Differentiating (11) with respect to time, the linear velocity can then be described as

$${}^{b_0}\dot{\mathbf{p}}_{C,i} = \begin{bmatrix} \dot{x} \\ \dot{y} \end{bmatrix} + \sum_{k=1}^{i-1}(2\,{}^{b_0}_{b_k}\dot{R}\;{}^{b_k}\mathbf{r}_c) + {}^{b_0}_{b_i}\dot{R}\;{}^{b_i}\mathbf{r}_c \tag{13}$$

where the angular velocity and differentiation of the rotation matrix for $i = \{2, \cdots, N\}$are as follows

$$\dot{\theta}_i = \dot{\theta}_1 + \sum_{k=1}^{i-1}\dot{\phi}_k \tag{14}$$

$${}^{b_0}_{b_i}\dot{R} = \begin{bmatrix} 0 & -\dot{\theta}_i \\ \dot{\theta}_i & 0 \end{bmatrix}{}^{b_0}_{b_i}R \tag{15}$$

For optimization, Section IV, the forward velocity of the snake robot is considered with respect to the robot's orientation (heading). This can be considered as the average of the link angles, where $\bar{\theta}_i \in \mathbb{R}$.

$$\bar{\theta} = \frac{1}{N}\sum_{i=1}^{N}\theta_i \tag{16}$$

Due to every link being of the same mass, the velocity at the CM of the snake robot in the global frame can be transformed to the body frame using the following relation,

$${}^{b_0}\dot{\mathbf{p}}_{C,i} = \begin{bmatrix} \dot{p}_x \\ \dot{p}_y \end{bmatrix} = \frac{1}{N}\sum_{i=1}^{N}{}^{b_0}_{b_i}R\begin{bmatrix} {}^{b_i}\dot{p}_{c,x} \\ {}^{b_i}\dot{p}_{c,y} \end{bmatrix} \tag{17}$$

The main contributor to forward velocity is the tangential component at the CoM in the body frame, $\bar{v}_t \in \mathbb{R}$, along the orientation of the robot, $\bar{\theta}$, represented by the following equation where subscript t denotes tangential.

$$\bar{v}_t = \dot{p}_y\cos(\bar{\theta}) - \dot{p}_x\sin(\bar{\theta}) \tag{18}$$

III. DYNAMICS

The dynamics of the snake robot, as shown in Fig. 2, with N links connecting $N-1$ revolute joints in addition to the antagonistic artificial-muscle-driven spring mechanism at each joint, was derived. The dynamic model neglects side-slip constraints (non-holonomic constraints) and assumes that anisotropic friction is applied at each link. Therefore, the robotic system has $N+2$ DOF. The forward dynamics of the snake robot were derived using Lagrangian mechanics.

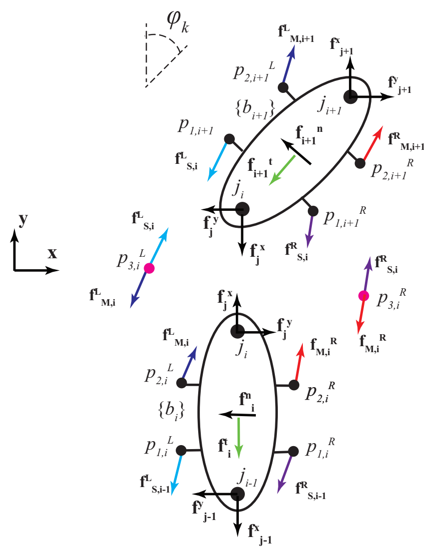

Fig. 3: The free body diagram of a module of the snake robot including the forces acting on the body of the snake robot.

A. Lagrangian of Artificial-Muscle-Driven Snake Robot

The generalized coordinates and generalized velocities $\mathbf{q} = [x, y, \theta_1, \phi_1, \cdots, \phi_{N-1}]^T$; $\dot{\mathbf{q}} = [\dot{x}, \dot{y}, \dot{\theta}_1, \dot{\phi}_1, \cdots, \dot{\phi}_{N-1}]^T$ will be found using forward dynamics based on the Lagrangian method as follows

$$T = \frac{1}{2}\sum_{i=1}^{N}(\mathbf{v}_i^T M \mathbf{v}_i + I_C\omega_i^2) \tag{19}$$

where $\mathbf{v}_i = {}^{b_0}\dot{\mathbf{p}}_{C,i}$, $\omega_i = \dot{\theta}_i$, $M \in \mathbb{R}^{N\times N}$ is the mass matrix, and $I_C \in \mathbb{R}^{N\times N}$ expressed in the body frame and will be I_{zz} is a matrix of the moment of inertia about the z-axis of rotation for each link.

No potential energy is considered due to the force of gravity, however, potential energy due to the tension springs of the system is considered by the following,

$$U = \frac{1}{2}k\sum_{i=1}^{N-1}((\Delta l_{s,i}^R)^2 + (\Delta l_{s,i}^L)^2) \tag{20}$$

corresponding to the change in length of the spring on the right (R) and left (L) sides of the links. The Euler-Lagrange equation can then be described as

$$\frac{d}{dt}\frac{\partial T}{\partial \dot{\mathbf{q}}_j} - \frac{\partial T}{\partial \mathbf{q}_j} + \frac{\partial U}{\partial \mathbf{q}_j} = \mathbf{Q}_j \tag{21}$$

where $j = \{1, 2, \cdots, N+2\}$ and with $\mathbf{Q}_j$ being the generalized and non-conservative forces.

B. Generalized and Non-Conservative Forces

The free body diagram of two-adjacent links is shown in Fig. 3. The forces and moments acting on each body can be categorized into four groups: 1) joint reaction forces, 2) friction forces, 3) muscle actuation forces (on the left and right sides of each body), and 4) non-conservative spring forces. The following equations are written for link $\{b_i\}$, note forces for other links can be found in a similar manner. The friction forces, normal and tangential, acting at the CM of the link with respect to the corresponding body frame can be written as follows

$$f_i^{f,n} = -\mu_n m_i g \frac{^{b_i}v_{i,x}}{|^{b_i}v_{i,x}|} \tag{22}$$

$$f_i^{f,t} = -\mu_t m_i g \frac{^{b_i}v_{i,y}}{|^{b_i}v_{i,y}|} \tag{23}$$

where the friction with the ground was modeled as Coulomb friction with anisotropic properties, $\mu_t \ll \mu_n$, where subscripts t and n denote tangential and normal directions. With $m_i, g, v_{i,x}, v_{i,y}$ representing the mass of a single link, gravitational acceleration, and the linear velocities at the CM acting in each component direction. The velocity vectors at the CM with respect to the body frame can be found by

$$\begin{bmatrix} ^{b_i}v_{i,x} \\ ^{b_i}v_{i,y} \end{bmatrix} = {}^{b_0}_{b_i}R^T \, \mathbf{v}_i \tag{24}$$

The friction forces are then translated with respect to the reference frame for consistency.

The torque about the connecting joint was generated from the use of a proportional-derivative (PD) controller which assisted with the derivation of the muscle actuation forces. The proportional-gain k_p and the derivative-gain k_d terms were taken as 29 and 1.2, respectively. The required torque was derived as follows

$$\tau_i = k_p(\phi_{i,d} - \phi_i) + k_d(\dot{\phi}_{i,d} - \dot{\phi}_i) \tag{25}$$

where $\phi_{i,d}$ and $\dot{\phi}_{i,d}$ are the desired joint angle and desired angular velocity given by,

$$\phi_{i,d} = \alpha \sin(\omega t) \tag{26}$$

$$\dot{\phi}_{i,d} = \alpha \, \omega \cos(\omega t) \tag{27}$$

where $\alpha = \frac{\pi}{12}$ rad, $\omega = \pi$ rad/s, and t as time in seconds. The muscle actuation forces can then be described as

$$\mathbf{f}_i^m = \frac{|\tau_i|}{\|^{b_0}\mathbf{r}_{m,i} \times \hat{\mathbf{e}}_i\|} \tag{28}$$

There are two methods for finding the spring forces which are dependent on which method is used for finding the connection of the muscle and spring, $^{b_0}\mathbf{p}_{3,i}$. The first method is from the reaction forces on the two bodies with relation to torque similar to the generation of the muscle forces. the second method is by the restoring force from the extension spring,

$$\mathbf{f}_i^s = \frac{|\tau_i|}{\|^{b_0}\mathbf{r}_{s,i} \times -\hat{\mathbf{e}}_i\|} = k(l_{s,i} - l_{s,0})\, \hat{\mathbf{e}}_i \tag{29}$$

where $^{b_0}\mathbf{r}_{m,i}, ^{b_0}\mathbf{r}_{s,i}$ are the moment arms from the muscle and spring respectively, to the connecting joint.

Therefore, the generalized and non-conservative forces term is as follows

$$\begin{aligned} \mathbf{Q}_j = &\sum_{i=1}^{N} (J_i^f(\mathbf{q}_j)^T \cdot \mathbf{f}_i^f) + \sum_{i=1}^{N-1} (J_i^m(\mathbf{q}_j)^T \cdot \mathbf{f}_i^m) \\ &+ \sum_{i=1}^{N-1} (J_i^s(\mathbf{q}_j)^T \cdot \mathbf{f}_i^s) \end{aligned} \tag{30}$$

where $J_i^f(\mathbf{q}_j) = \frac{\partial\, ^{b_0}_{i-1}\mathbf{p}_C}{\partial \mathbf{q}_j}$, $J_i^m(\mathbf{q}_j) = \frac{\partial\, ^{b_0}\mathbf{p}_{2,i}}{\partial \mathbf{q}_j}$, and $J_i^s(\mathbf{q}_j) = \frac{\partial\, ^{b_0}\mathbf{p}_{1,i+1}}{\partial \mathbf{q}_j}$ are the Jacobian matrices at the center of mass of each link and the two attachment points corresponding to the locations of where each of the forces are acting upon.

C. Equations of Motion

Substituting (19), (20), (30) into (21) yields the following equations of motion

$$\begin{aligned} M(\mathbf{q})\ddot{\mathbf{q}} + \mathbf{c}(\mathbf{q}, \dot{\mathbf{q}}) = &J_i^f(\mathbf{q}_j)^T \cdot \mathbf{f}_i^f + J_i^m(\mathbf{q}_j)^T \cdot \mathbf{f}_i^m \\ &+ J_i^s(\mathbf{q}_j)^T \cdot \mathbf{f}_i^s \end{aligned} \tag{31}$$

where $M(\mathbf{q})$ is a symmetric and positive-definite mass matrix and $\mathbf{c}(\mathbf{q}, \dot{\mathbf{q}})$ is the nonlinear acceleration expressions including centrifugal and Coriolis terms.

D. Dynamic Related Cases of Snake Movement

As a result of having three methods of finding the location of the mid-point between the muscle and the spring, $^{b_0}\mathbf{p}_{3,i}$, relating to joint torque, muscle length, and joint angle, six cases emerge to describe the dynamics of the system.

When the muscle is passive during free extension there is no work being done by the muscle which results in the muscle force being zero. However, force is generated from the coupled extension spring. For this reason using the balance of forces approach from (9) is not feasible. We instead use the reaction forces of the muscle and springs acting in series on the bodies to determine the spring force as a response to torque, see (29). Then by using the second relation from (29), we can solve for the spring length. With this, (8) can be used to find the location of $^{b_0}\mathbf{p}_{3,i}$. Once the muscle has returned to its initial length while still passive, method 1 (7) can be used to find $^{b_0}\mathbf{p}_{3,i}$. It is only when the muscle is active that the third method (9) can be used.

IV. VELOCITY-BASED DESIGN OPTIMIZATION

Following the formulation of the dynamic model, a velocity-based design optimization was done to improve the snake robot's velocity. The tangential velocity along the robot's orientation is the main contributor to the forward velocity. Previous studies show the geometrical design aspect greatly impacted the robot's forward velocity [13]–[15], therefore, the following parameters $h_1, h_2, w, l_m, l_s, k, m$ were selected for the design optimization. Consider the following optimization problem of maximizing $\bar{v}_t(\mathbf{x})$ in (18), subjected to,

$$
\begin{aligned}
h_2 - \frac{h_1}{2} &\le 0 \qquad\qquad (32)\\
2h_2 - l_{m,0} - l_{s,0} &= 0\\
l_{b,j} \le x_j &\le u_{b,j} \qquad x_j \in \mathbf{x}\\
-|\bar{v}_t(\mathbf{x})| &< 0\\
{}^{b_i}v_n^i(\mathbf{x}) &= 0
\end{aligned}
$$

where $\mathbf{x} \in \mathbb{R}^7$ is the optimization variable vector defined as, $\mathbf{x} = [h_1, h_2, w, l_m, l_s, k, m]^T$, and the objective function is defined by the velocity component along the orientation of the snake robot, $\bar{v}_t(\mathbf{x})$. The objective function is subjected to a series of constraints, (32), including the nonlinear inequality constraint on the placement of the two attachments that connect the spring and muscle to each body. Additionally, there is a linear equality constraint to ensure that at rest the lengths of the muscle and spring should be the distance from one attachment to the other for the links to be aligned with each other. There is a nonlinear inequality constraint for the forward velocity to remain positive and there is a nonlinear equality constraint on the velocity in the normal direction with respect to each link to avoid any side-slip.

MATLAB's nonlinear solvers 'fmincon' and 'patternsearch' were used to maximize $\bar{v}_t(\mathbf{x})$. The components of vector $\mathbf{x}$ are bounded by lower and upper bound values, $l_b = [75.0, 15.0, 15.0, 30.0, 7.9, 0.04, 0.06]^T$ and $u_b = [150.0, 75.0, 30.0, 80.0, 25.0, 1.0, 0.12]^T$, respectively. Note the units are (mm) for the first five terms, (N/mm) for 6th term, and (kg) for the last term.

V. EXPERIMENTAL SETUP

The experiment setup shown in Fig. 4a consisted of a camera, the electronic circuitry including 2-way and 3-way valves that would activate the muscles, a 6V power supply, and the wheeled two link module robot shown in Fig. 4b. There is no controlling of the pressure by the 2-way or 3-way valves. The analytic and annotation tool Kinovea (0.9.5) was used to track the link and joint angles, as well as the positions of the two attachment points and muscle-spring connecting point on either side of the body, Fig. 4c.

VI. RESULTS AND DISCUSSION

Three sets of data were compared for the joint position, Fig. 5b, the desired ϕ_d set to be used in the torque controller, the theoretical ϕ from the dynamic model, and the raw experimental ϕ_{exp}. Tuning the torque PD controller, the desired angle was made to follow the trajectory of the experiment. The reference is used to match the actual joint angle from the dynamic model with the experimental data.

Only the right muscle and spring lengths' results are shown in Fig. 5c-d. Between the experiment and simulation there was noticeably more contraction in the actual muscles compared to the model. Although the spring lengths were similar in average magnitude, the pattern differed. The muscles act antagonistically to each other where the left muscle is activated first and is also the last to deactivate. At both start and end time, the left muscle has no force resistance from the right one because the right side is deactivated, therefore there is a spike at these times in the results.

TABLE I: Velocity-Based Optimization

Parameters	*Optimal Values* fmincon	*Optimal Values* patternsearch	*Current Values*
h_1(mm)	111.4	75.0	111.4
h_2 (mm)	40.7	37.5	40.7
w (mm)	25.97	25.97	25.97
l_m (mm)	66.4	63.2	66.4
l_s (mm)	15.0	11.8	15.0
k (N/mm)	0.464	0.464	0.464
m (kg)	0.082	0.082	0.082

It is important to note that because a PD controller was implemented to generate the needed torque in the dynamic model and there was no controller used for the experiment the lengths for the muscle and spring differ. In the future the intake pressure of the actuators for the experiment will be controlled to gradually insert and exhaust air to and from the muscles resulting in clearer data.

A dynamics-based design optimization was performed to maximize the robot's forward velocity, Fig. 5e. Table I shows that after optimizing the links' geometric parameters the maximum velocity for the 2-link robot was obtained. Using fmincon, the parameters did not change from the initial design resulting in an optimal velocity of 520.5 mm/s. A second solver 'patternsearch' was used to verify that the global minimum was obtained rather than a local one. The optimized parameters changed to some degree, yielding 520.6 mm/s optimal velocity, which is a significant improvement from the current model with 323.8 mm/s max velocity. Although the velocity did not change between the two solvers, unlike with the first solver, the second solver resulted in a different set of parameters from the current. It is important to note that 'patternsearch' went through five times the number of iterations from 'fmincon'.

Future work will include an N-link dynamic modeling in the velocity-based optimization. An energy-velocity based optimization will be performed to obtain the greatest velocity with the least amount of energy consumption. The underlying characteristics of the PAMs will also be explored.

ACKNOWLEDGMENT

First author, Ms. Ayla Valles, has been supported by the New Mexico Space Grant Consortium (NMSGC) Fellowship through a NASA Cooperative Agreement No. NM-80NSSC20M0034.

REFERENCES

[1] K. Osuka and H. Kitajima, "Development of mobile inspection robot for rescue activities: Moira," in *Proceedings 2003 IEEE/RSJ International Conference on Intelligent Robots and Systems (IROS 2003)(Cat. No. 03CH37453)*, vol. 4. IEEE, 2003, pp. 3373–3377.

[2] J. Borenstein, M. Hansen, and A. Borrell, "The omnitread ot-4 serpentine robot—design and performance," *Journal of Field Robotics*, vol. 24, no. 7, pp. 601–621, 2007.

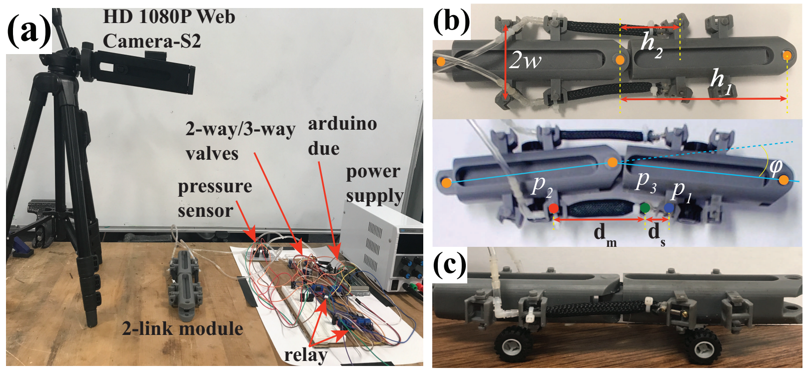

Fig. 4: (a) Experimental setup and electronic components, (b) experimental demonstration, (c) 2-link module.

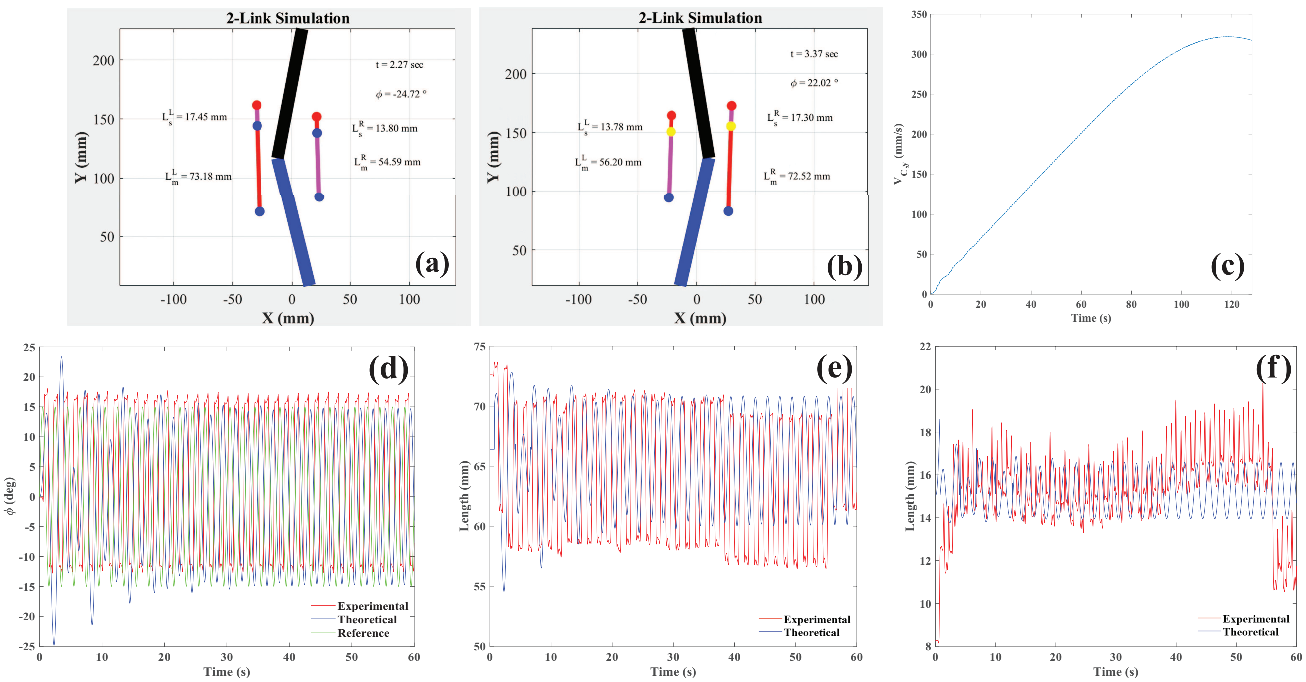

Fig. 5: Dynamic simulation and experimental results comparison of a wheeled 2-link module, (a,b) simulated representation, (c) global forward velocity along orientation of robot, (d) joint angle, (e,f) muscle and spring lengths respectively.

[3] S. Davis, N. Tsagarakis, J. Canderle, and D. G. Caldwell, "Enhanced modelling and performance in braided pneumatic muscle actuators," *The International Journal of Robotics Research*, vol. 22, no. 3-4, pp. 213–227, 2003.

[4] J. Zhang, J. Sheng, C. T. O'Neill, C. J. Walsh, R. J. Wood, J.-H. Ryu, J. P. Desai, and M. C. Yip, "Robotic artificial muscles: Current progress and future perspectives," *IEEE transactions on robotics*, vol. 35, no. 3, pp. 761–781, 2019.

[5] J. Schroder, D. Erol, K. Kawamura, and R. Dillman, "Dynamic pneumatic actuator model for a model-based torque controller," in *Proceedings 2003 IEEE International Symposium on Computational Intelligence in Robotics and Automation. Computational Intelligence in Robotics and Automation for the New Millennium (Cat. No. 03EX694)*, vol. 1. IEEE, 2003, pp. 342–347.

[6] Z. Guo and L. Mahadevan, "Limbless undulatory propulsion on land," *Proceedings of the National Academy of Sciences*, vol. 105, no. 9, pp. 3179–3184, 2008.

[7] B. C. Jayne, "Muscular mechanisms of snake locomotion: an electromyographic study of the sidewinding and concertina modes of crotalus cerastes, nerodia fasciata and elaphe obsoleta," *Journal of Experimental Biology*, vol. 140, no. 1, pp. 1–33, 1988.

[8] ——, "Muscular mechanisms of snake locomotion: an electromyographic study of lateral undulation of the florida banded water snake (nerodia fasciata) and the yellow rat snake (elaphe obsoleta)," *Journal of Morphology*, vol. 197, no. 2, pp. 159–181, 1988.

[9] B. R. Moon and C. Gans, "Kinematics, muscular activity and propulsion in gopher snakes," *Journal of Experimental Biology*, vol. 201, no. 19, pp. 2669–2684, 1998.

[10] J. Gray, "The mechanism of locomotion in snakes," *Journal of experimental biology*, vol. 23, no. 2, pp. 101–120, 1946.

[11] D. D. Arachchige, D. M. Perera, S. Mallikarachchi, I. Kanj, Y. Chen, and I. S. Godage, "Wheelless soft robotic snake locomotion: Study on sidewinding and helical rolling gaits," in *2023 IEEE International Conference on Soft Robotics (RoboSoft)*. IEEE, 2023, pp. 1–6.

[12] F. Rozaidi, E. Waters, O. Dawes, J. Yang, J. R. Davidson, and R. L. Hatton, "Hissbot: Sidewinding with a soft snake robot," in *2023 IEEE International Conference on Soft Robotics (RoboSoft)*. IEEE, 2023, pp. 1–7.

[13] M. Lopez and M. Haghshenas-Jaryani, "A muscle-driven mechanism for locomotion of snake-robots," *Automation*, vol. 3, no. 1, pp. 1–26, 2021.

[14] M. Haghshenas-Jaryani, "Dynamics and computed-muscle-force control of a planar muscle-driven snake robot," in *Actuators*, vol. 11, no. 7. MDPI, 2022, p. 194.

[15] M. Lopez and M. Haghshenas-Jaryani, "A study of energy-efficient and optimal locomotion in a pneumatic artificial muscle-driven snake robot," *Robotics*, vol. 12, no. 3, p. 89, 2023.